K. Dang Van, G. Cailletaud,† J. F. Flavenot,‡ A. Le Douaron,§ and H. P. Lieurade¶*

Criterion for High Cycle Fatigue Failure Under Multiaxial Loading

REFERENCE Dang Van, K., Cailletaud, G., Flavenot, J. F., Le Douaron, A., and Lieurade, H. P., **Criterion for high cycle fatigue failure under multiaxial loading,** *Biaxial and Multiaxial Fatigue*, EGF 3 (Edited by M. W. Brown and K. J. Miller), 1989, Mechanical Engineering Publications, London, pp. 459–478.

ABSTRACT Industrial structures undergoing fatigue stress are most often subjected to complex loading patterns. The design of such structures is generally based upon existing fatigue criteria which do not make it possible to take into account the type of complex loading involved.

The aim of this study is to describe a three-dimensional criterion relative to fatigue endurance. This criterion is compared with other fatigue criteria. The experimental verification of the criterion is then carried out for different metals (steels, cast iron, light alloys, etc.).

Finally, the application of the proposed criterion is examined for the case of industrial structures subjected to complex loads.

Introduction

Fatigue crack initiation is a macroscopic phenomenon taking place on a scale of the order of the grain size or a few grain diameters. At this scale, the material is neither homogeneous nor isotropic and local responses can differ significantly from macroscopic values resulting from calculations or from measurements by engineers. What the engineer perceives is already 'filtered', as it were, by the structure composed of macro-elements, corresponding, for example, to the size of the strain gauge, and even more so to the test specimen. For this reason, a direct approach based upon experiments correlated by macroscopic parameters may be insufficient. Without going down, as in certain theories, to the level of dislocations (**1**), it would be better to derive macroscopic rules, to postulate the initiation criterion at the level of local microscopic variables in the apparently stabilized state, even if this requires proposing a procedure for calculating them from the usual macroscopic parameters of the engineer. This approach, which is in theory more complicated, nevertheless offers a certain number of significant advantages.

Dang Van originally proposed this approach in (**1**) and (**2**). The theoretical basis of his criterion is extensively developed in (**3**). For the first time, the

* Ecole Polytechnique, LMS–91128 Palaiseau Cedex, France.
† Centre des Matériaux de l'Ecole des Mines de Paris, BP 87, 91003 Evry Cedex, France.
‡ CETIM, 52 Avenue Félix Louat, 60300 Senlis Cedex, France.
§ RNUR, 8–10 Avenue Emile Zola, 92109, Boulogne Billancourt Cedex, France.
¶ IRSID, 185 rue du Président Roosevelt, 78105 Saint Germain en Laye Cedex, France.

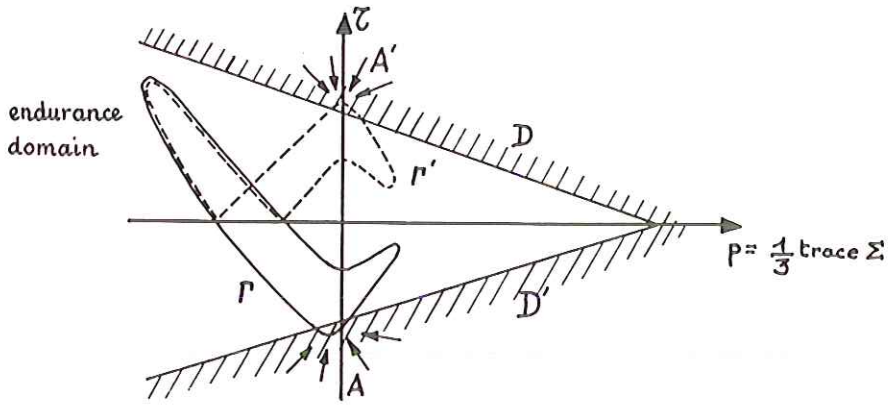

Fig 1 Dang Van criterion. Endurance domain and complex loading path

proposed criterion is set out using the current microscopic stress variables calculated at each time, based on the macroscopic stress cycle (engineering stresses).

In particular, fatigue failure occurs when, at a given time, the combination $\{\tau(t), p(t)\}$ (where τ is the local shear stress and p the hydrostatic stress) cuts the convex which defines the endurance domain. In fact, this endurance domain is bordered by two straight lines whose equation is (see Fig. 1)

$$f(\sigma) \equiv \tau \pm ap \mp b = 0 \tag{1}$$

As defined in this approach, various criteria involve two parameters. A review of this criterion is given in (**4**).

Comparison of different damage criteria

In this paragraph we compare the model proposed by Dang Van with two other models: those of Sines (**5**) and Crossland (**6**). For the latter two criteria, we of course consider a formulation derived from Fuchs' idea (**7**) which is valid for complex loading.

The purpose of this comparison is to show the differences of one model from the other, and to propose tests which may lead to the elimination of one of them for a given material. For this we begin by identifying the free coefficients of each model so that the results obtained are identical in alternating tension–compression and repeated tension–compression: these tests, simple to perform, can serve as a certain reference. We shall then examine the response of the models for different types of two-dimensional loading in plane stress, in phase and out of phase.

Form adopted for each model

We shall designate here σ_1 as the fatigue limit under alternating tension–compression, and we shall assume that the variation in the fatigue limit is a linear function of the mean stress under tension–compression

$$\sigma_a = \sigma_1(1 - b\sigma_m) \tag{2}$$

(σ_a = alternating stress permissible for mean stress, σ_m, and b characteristic of the material).

The fatigue limit under undulating tension σ_1' is written as follows for these conditions

$$\sigma_1' = \sigma_1/(1 + b\sigma_1) \tag{3}$$

Now the Sines criterion involves a linear combination of the mean hydrostatic stress of the cycle (p_{mean}) and of the maximum of the range of second invariant (ΔJ_2)

$$\tfrac{1}{2}\Delta J_2 = A + Bp_{mean}$$

where

$$\Delta J_2(t_1, t_2) = J_2\{\sigma_{ij}(t_1) - \sigma_{ij}(t_2)\}$$

We thus find, respectively, under alternating and repeating tension

$$\sigma_1 = A + B \times 0$$

and

$$\sigma_1'/2 = \mathrm{A} + \mathrm{B}\sigma_1'/6 \tag{4}$$

From this we obtain the criterion:

$$\tfrac{1}{2}\Delta J_2 = \sigma_1(1 - 3bp_{mean}) \tag{5}$$

Alternatively, to obtain the expression of Crossland's criterion, one need only replace the mean value of the hydrostatic stress by its maximum value. This gives:

Under alternating tension

$$\sigma_1 = A + B\sigma_1/3 \tag{6}$$

Under repeated tension

$$\sigma_1'/2 = A + B\sigma_1'/3$$

So that, finally

$$\Delta J_2/2 = \sigma_1(1 - 3bp_{max})/(1 - b\sigma_1) \tag{7}$$

Dang Van's criterion is expressed similarly as a function of the maximum

local shear stress amplitude and of p (but involves current values and not average or maximum values), i.e.

$$\tau(t) = A + Bp(t) \tag{8}$$

The following values are obtained, respectively, under alternating and repeated tension

$$\sigma_1/2 = A + B\sigma_1/3$$

and

$$\sigma_1'/4 = A + B\sigma_1'/3 \tag{9}$$

so that

$$\tau(t) = \sigma_1\{1 - 3b + p(t)\}/2(1 - b \cdot \sigma_1) \tag{10}$$

Application of fatigue criteria to simple loading

We shall be dealing here with the case of plane stresses, $\sigma_3 = 0$ and $\sigma_2 = k\sigma_1$, assuming that the loading is either alternating or repeated. The values obtained for the most characteristic loadings are given in Table 1, and the curves corresponding to the fatigue limit are shown in Fig. 2.

Table 1 contains several interesting elements. For example, it is known that a mean torsion has no effect on the fatigue limit, which is shown here by the fact that the torsion amplitude is the same under alternating and repeated loading, for all criteria.

Also, the Sines criterion calls for a fixed ratio of $\sqrt{3}$ between the fatigue limit under alternating tension and that obtained under alternating torsion, which may be a drawback. However, for the other two criteria, the variation of this ratio is obtained through the coefficient, b, which also gives the influence of the mean stress: this dual role is also liable to raise problems.

Table 1 Comparison of endurance limits for various loading modes, predicted by three failure criteria (plane stress state)

Loading mode	R	*Criterion*		
		Sines	*Crossland*	*Dang Van*
Tension	−1	σ_1	σ_1	σ_1
Torsion		$\sigma_1/\sqrt{3}$	$\sigma_1/\sqrt{3}(1 - b\sigma_1)$	$\sigma_1/2(1 - b\sigma_1)$
Equibiaxial tension		σ_1	$\sigma_1/(1 + b\sigma_1)$	$\sigma_1/(1 + b\sigma_1)$
Tension	0	$2\sigma_1/(1 + b\sigma_1)$	$2\sigma_1/(1 + b\sigma_1)$	$2\sigma_1/(1 + b\sigma_1)$
Compression		$2\sigma_1/(1 - b\sigma_1)$	$2\sigma_1/(1 - b\sigma_1)$	$2\sigma_1/(1 - b\sigma_1)$
Biaxial tension		$2\sigma_1/(1 + 2b\sigma_1)$	$2\sigma_1/(1 + 3b\sigma_1)$	$2\sigma_1/(1 + 3b\sigma_1)$
Biaxial compression		$2\sigma_1/(1 - 2b\sigma_1)$	$2\sigma_1/(1 - b\sigma_1)$	$2\sigma_1/(1 - b\sigma_1)$
Torsion		$2\sigma_1/\sqrt{3}$	$2\sigma_1/\sqrt{3}(1 - b\sigma_1)$	$\sigma_1/(1 - b\sigma_1)$

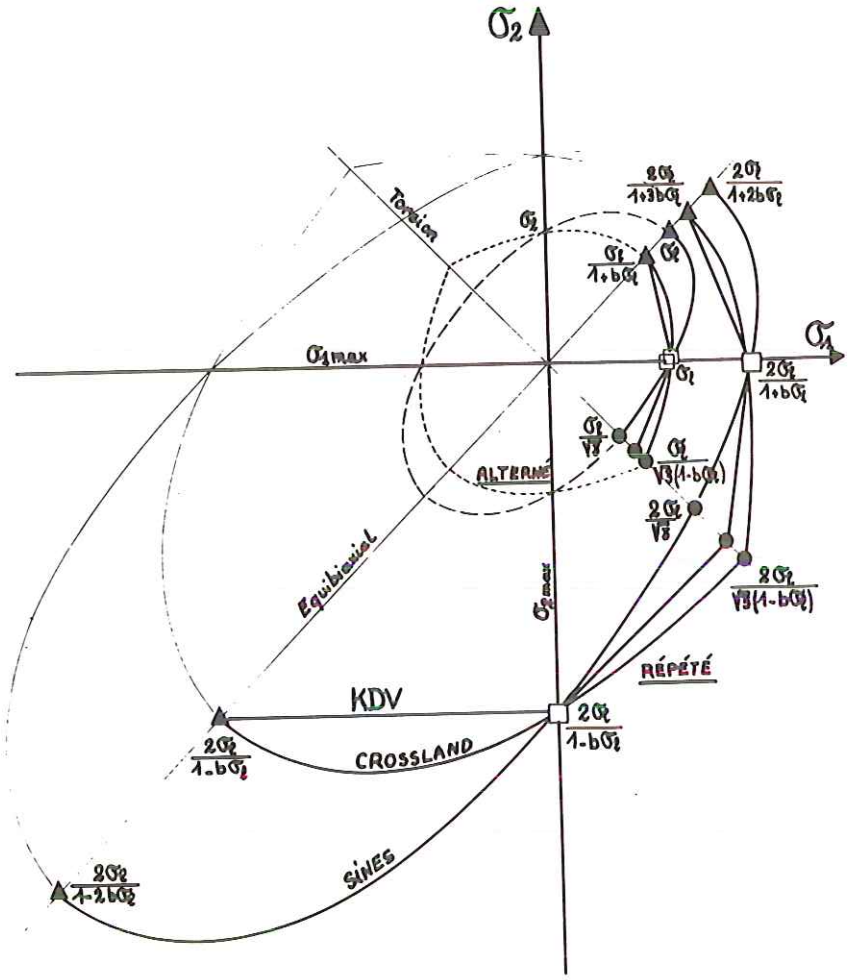

Fig 2 Comparison of various criteria for typical loadings (plane stress state)

The results obtained by the Crossland and Dang Van criteria are identical, except under torsion, owing to the differences between the second invariant and the shear stress.

Finally, it should be noted that the curves obtained are ellipses for the Sines and Crossland criteria and straight segments for the Dang Van criterion.

Use of tension–torsion models for out of phase loading

The out-of-phase tension–torsion test is one of the most interesting tests, and can be carried out by means of hydraulically controlled TTC (torsion + tension–compression) machines. Using thin-walled tubes, it is thus possible to

impose on a volume element an alternating load for each component, but with a constant equivalent stress (second invariant), for example.

We are thus considering here the case of alternating loading in which all the stresses are zero except

$$\sigma_{11} = \sigma = \sigma_M \cos \omega t$$
$$\sigma_{12} = \tau = \tau_M \sin \omega t \qquad (11)$$

Under these conditions, it is easy to show that J_2 depends on the relative values of the shear stress and the tension and is equal to Max $(\sigma_M, \sqrt{3}\tau_M)$; the mean value of the hydrostatic pressure is of course zero, its maximum value being equal to $1/3\sigma_M$. There are thus two possible cases for the application of the Sines and Crossland criteria

(i) $\sigma_M \geq \sqrt{3}\tau_M$; the two criteria give $\sqrt{3}\tau_M \leq \sigma_M = \sigma_I$

(ii) $\sigma_M \leq \sqrt{3}\tau_M$; the Sines criterion is written simply

$$\sigma_M \leq \sqrt{3}\tau_M = \sigma_I$$

whereas the Crossland criterion leads to a linear variation between σ_M and τ_M, namely

$$\sqrt{3}\tau_M + \{b \cdot \sigma_I/(1 - b \cdot \sigma_I)\}\sigma_M = \sigma_I/(1 - b \cdot \sigma_I) \qquad (12)$$

The application of the Dang Van criterion requires the search for the facet for which the quantity $\{\tau + (3b\sigma_I p)/2(1 - b\sigma_I)\}$ is at its maximum during the cycle: for this, we consider the plane $z = 0$ which contains the maximum shear stresses. We find in particular the normal n_1 which characterizes a plane for which the shear stress is equal to τ and the normal n_2 corresponding to a plane in which τ has no influence (Fig. 3). The plot of the loading in the diagram $(\tau, 3p)$ for a plane whose normal forms an angle of φ with n_1 is an ellipse with an inclined axis having the equation

$$\tau = \{\sigma_M^2 - (3p)^2\}^{1/2} \cdot (\tau_M/\sigma_M) \cos 2\varphi + (3p/2) \sin 2\varphi \qquad (13)$$

We obtain an ellipse with horizontal and vertical axes when $\varphi = 0$ (normal n_1), and an ellipse degenerated into straight-line segments when $\varphi = \pi/4$ (normal n_2). The value obtained by the criterion will be at the point of concurrence of this ellipse and of the critical line given by equation (8).

The analytical study of this intersection shows two cases.

(i) If $\tau_M \leq \sigma_M/2\sqrt{(1 - b\sigma_I)}$, $2\sqrt{(1 - b\sigma_I)}\tau_M \leq \sigma_M = \sigma_I$

the critical plane is the plane (2) characterized by $\varphi = \pi/4$. It is noted that, for $\sigma_M/2 \leq \tau_M/2\sqrt{(1 - b\sigma_I)}$, this plane is not the one which experiences the maximum shear stress amplitude; it is greater on plane (1), for example.

(ii) If $\tau_M \geq \sigma_M/2\sqrt{(1 - b\sigma_I)}$, the relationship between the critical values of τ_M and of σ_M is of the fourth degree

$$16(1 - b\sigma_I)^2\tau_M^4 + 4(2b\sigma_I - 1)\tau_M^2 \cdot \sigma_M^2 - 4\sigma_I^2 \cdot \tau_M^2 + \sigma_I^2 \cdot \sigma_M^2 = 0 \qquad (14)$$

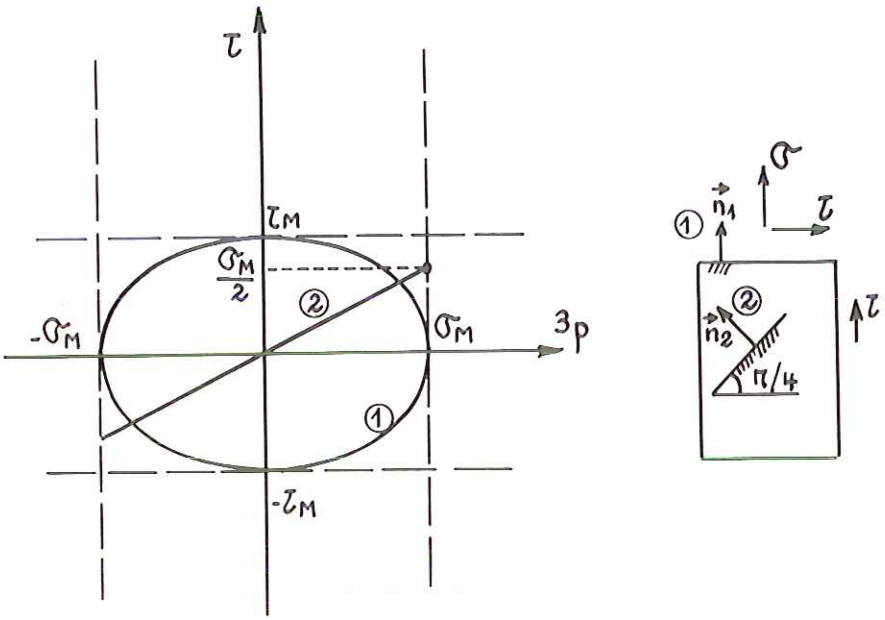

Fig 3 Plotting of loading cycles corresponding to two specific planes in out-of-phase tension–torsion (Dang Van diagram)

and the angle formed by the normal to the critical plane and n_1 is

$$\varphi = \tfrac{1}{2}\arcsin\,[b\sigma_1/(1 - b\sigma_1)\cdot\{(2\tau_M/\sigma_M)^2 - 1\}] \qquad (15)$$

Figure 4 shows the variations of this critical plane as a function of the load ratio τ_M/σ_M. It corresponds to the plane (2) for low shear stresses and tends towards the plane (1) for low tension values. Also shown is the plane for which the shear stress amplitude is at its maximum (characterized by φ).

The results obtained by the three criteria are shown in Fig. 5. Also shown is the critical curve obtained with the Dang Van criterion introducing the second invariant, which is characterized by

$$\sigma_M = \sigma_1$$

if

$$\sqrt{\{3(1 - b\cdot\sigma_1)\}}\cdot\tau_M \leq \sigma_M$$

$$9(1 - b\cdot\sigma_1)^2\cdot\tau_M^4 + 3(2b\cdot\sigma_1 - 1)\cdot\tau_M^2\cdot\sigma_M^2 - 3\sigma_1^2\cdot\tau_M^2 + \sigma_1^2\cdot\sigma_M^2 = 0 \qquad (16)$$

if

$$\sqrt{\{3(1 - b\cdot\sigma_1)\}}\cdot\tau_M \geq \sigma_M$$

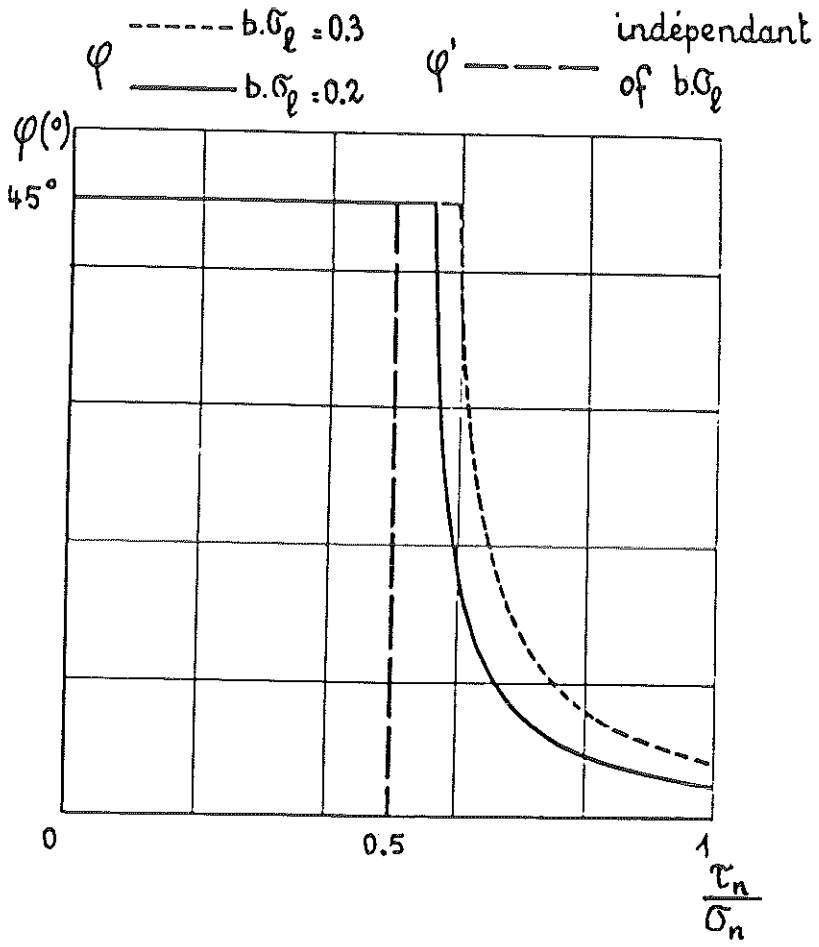

Fig 4 Evolution of the angle between the critical plane and the horizontal line in out-of-phase tension–torsion loading, as a function of the ratio between shear and tension stresses (Dang Van criterion)

The results show that there is little or no interaction between components (Sines), i.e., it is practically necessary to obtain the tension or torsion fatigue limit in order to obtain failure data under out-of-phase tension–torsion: adding a small torsion signal out of phase with a tension signal does not alter in any way the fatigue limit. This independence of components, not found experimentally with low-cycle fatigue, doubtless owing to plastic flow, should be verified for high-cycle fatigue.

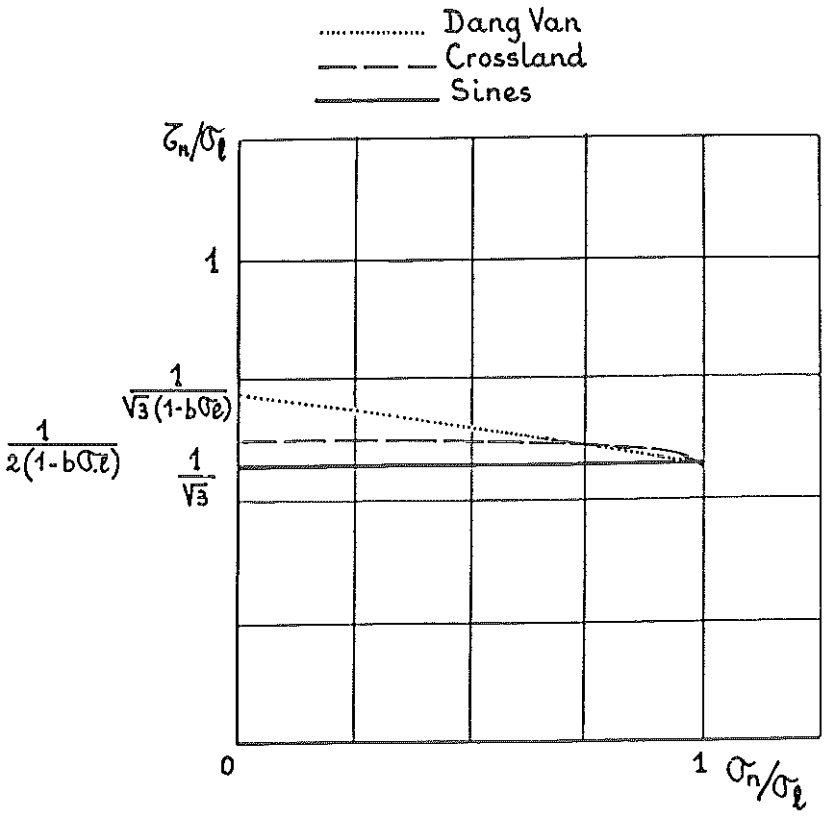

Fig 5 Out of phase (90 degrees) tension–torsion loading – drawing of the critical curves evaluated by various criteria for $b\sigma_1 = 0.2$

Use of models for out of phase 'equibiaxial' tension

It is now assumed that the only non-zero stresses are

$$\sigma_{11} = \sigma_1 = \sigma_a \cos \omega t$$

and (17)

$$\sigma_{22} = \sigma_2 = \sigma_a \sin \omega t$$

In this case, the evaluation of critical quantities for the Sines and Crossland criteria leads to

$$\frac{\Delta J_2}{2} = \sqrt{(3/2)}\sigma_a$$

$$p_{mean} = 0$$

$$p_{max} = (2/3)\sigma_a \tag{18}$$

and the fatigue limits obtained are:
for the Sines criterion

$$\sigma_a = \sqrt{(2/3)}\sigma_1$$

and for the Crossland criterion

$$\sigma_a = \sqrt{2}\sigma_1/\{\sqrt{3} + b\sigma_1(2 - \sqrt{3})\} \tag{19}$$

The load paths in the plane τ, p on two types of plane are indicated in Fig. 6. It is noted that the critical plane will be different for low or high values of the slope $b\sigma_1/2(1 - b\sigma_1)$ of the critical line. However, for usual values (obtained for example with $b\sigma_1 = 0.2$), it is the plane (2) which is relevant. The limit value found in this case is

$$\sigma_M = \sigma_1/\{2(2b^2\sigma_1^2 - 2b\sigma_1 + 1)\}^{1/2} \tag{20}$$

It is thus observed here that the introduction of current shear stress and hydrostatic pressure values leads to a smaller reduction in the fatigue life with the Dang Van criterion. With $b\sigma_1 = 0.2$, we find, respectively, with the Crossland, Sines, and Dang Van criteria, $0.79\sigma_1$, $0.82\sigma_1$, and $0.86\sigma_1$.

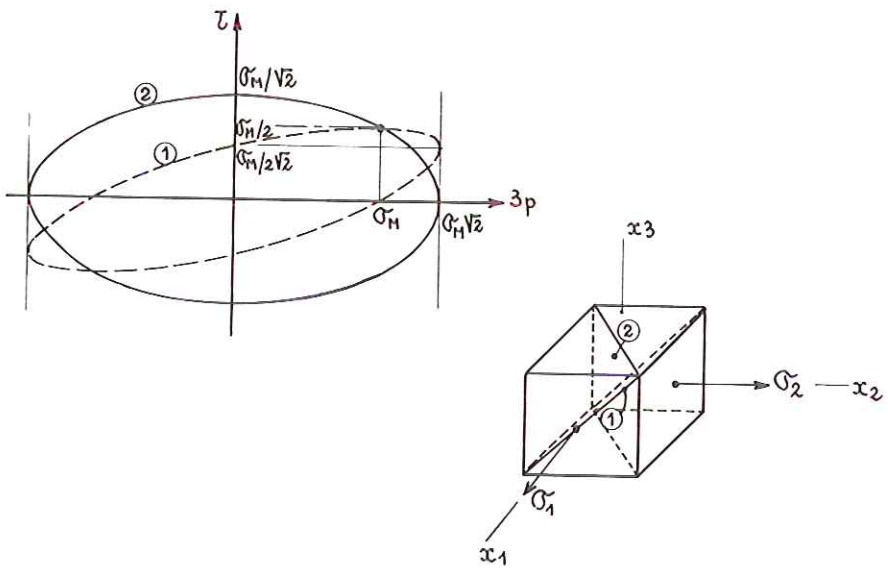

Fig 6 Loading cycle in the (τ, $3p$) diagram for the out-of-phase equibiaxial stress in tension: (1) 1st bisectrix of plane 2–3; (2) 1st bisectrix of plane 1–2

Use of models in equibiaxial shear stress out of phase

If now we assume that the only nonzero terms of stress tensor are $\sigma_{12} = \sigma_{21} = \tau_M \cos \omega t$ and $\sigma_{23} = \sigma_{32} = \tau_M \sin \omega t$, we are dealing, on the plane (1) having the normal (1, 0, 0), with a shear stress having a constant modulus covering successively all the directions of the plane. We then find

$$\Delta J_2/2 = \sqrt{3}\tau_M \quad \text{and} \quad p_{max} = p_m = 0 \tag{21}$$

Placed in their respective formulas, these values lead quite simply to the values obtained under simple shear stress $\sigma_1/3$, according to Sines, and $\sigma_1/3(1 - b\sigma_1)$, according to Crossland.

The same result is obtained with the Dang Van criterion, whereby the critical plane (1) sees a maximum shear stress amplitude of τ_M, leading to $\tau_M = \sigma_1/2(1 - b\sigma_1)$.

A summary of comparisons

The comparison of different damage criteria leads to the following observations.

(i) The greatest differences between adjusted criteria for alternating and repeated tension are found under simple torsion.

(ii) For out of phase loading, all the models considered here indicate no influence of the second component in the case of two shear stress components, a significant influence for two tension components and a small influence with a shear stress and a tension.

Experimental verification of the Dang Van criterion

Experimental study

Different grades of steel, cast iron, and light alloys were investigated. Tests were carried out on specimens loaded by fatigue machines at frequencies between 40 and 100 Hz.

In each case, the endurance limit was determined by means of the staircase method, a specimen being considered uncracked if it reached 10^7 or 10^8 cycles without failure.

Table 2 groups the mechanical properties of the materials investigated as well as the results obtained in reference (**8**).

Application of the Dang Van criterion

For the different cases examined, the shear stress amplitude τ and the hydrostatic stress p were calculated. Table 3 indicates the calculation phases in the case of cyclic uniaxial tension loads and torsion loads.

Table 2 Endurance limit ($N \geqq 10^7$ cycles) and parameters a and b from $\tau_a = a - b \cdot p$ for various materials

Material	σ_Y (*MPa*)	*UTS* (*MPa*)	*Loading mode*	R	σ_D, τ_D (*MPa*)	a	b $(MPa)^{-1}$
35 CD 4	935	1050	Tension	−1.75	550	0.39	310
				−1	525		
				0	395		
				0.2	405		
			Biaxial tension ($\sigma_2/\sigma_1 = 0.3$)	0	320		
			Torsion	−1	315		
				0	305		
E 36	400	600	Tension	−1	285	0.35	166
				0	210		
			Torsion	−1	155		
				0	160		
Rail steel	410	760	Tension	−∞	358	0.42	195
				−1	328		
				0	258		
			Torsion	−1	187		
				0	196		
AU 4 G	380	480	Tension	−1	130	0.36	80
			Torsion	−1	80		
ASG 03	70	155	Tension	−1	70	1.06	55
			Torsion	−1	55		
20 MB 5	995	1055	Tension	−1	600	0.43	265
			Torsion	−1	265		
Ferritic cast iron	330	480	Tension	−1	270	1.05	180
			Torsion	−1	180		
Pearlitic cast iron	400	550	Tension	−1	300	1.20	205
			Torsion	−1	205		

Figures 7 and 8 give the test results obtained, respectively, on a steel grade 35 CD4 and on a rail steel. The levels of the parameters a and b of the relationship

$$\tau + ap = b \tag{22}$$

are provided in Table 2.

In the case of the steel 35 CD4 for which the Wöhler curve was determined, for each type of loading, damage lines for 10^7, 10^6, and 10^5 cycles were plotted (Fig. 7). When the fatigue life decreases, there is a substantial decrease in a at the same time as an increase in b.

Allowance for residual stresses

The stress condition resulting from fatigue loading may be uniaxial; the residual stress condition is always multiaxial. When the designer of a mechanical component containing residual stresses wishes to predict the fatigue strength of the component, he must apply a calculation criterion.

Based upon fatigue test results and stabilized residual stresses for induction-hardened parts, it has been possible to show that the Dang Van criterion accounts correctly for fatigue behaviour in the presence of residual stresses.

Table 3 Use of the Dang Van criterion in the case of simple loading

$\sigma(t) = \sigma_a \sin \omega t$
$p = \frac{1}{3}(\sigma_1 + \sigma_2 + \sigma_3)$
$\tau_a = T(t) - T_0$

$\sigma_1, \sigma_2, \sigma_3$: principal stresses
$T(t)$: macroscopic shear stress
$T_0 = \frac{1}{2}(T_{max} + T_{min})$ = mean shear stress

Loading	*Sketch*	*Stresses*	*Instantaneous values*	*Extrema*
Uniaxial stress	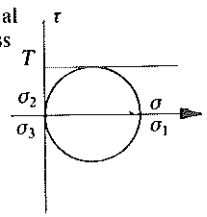	σ_1 $\sigma_2 = \sigma_3 = 0$ $T = \sigma_{1/2}$	$p(t) = \frac{1}{3}(\sigma_m + \sigma_a \sin \omega t)$ $\tau(t) = \frac{1}{2}\sigma_a \sin \omega t$ $\tau_a = \frac{3}{2}p - (\sigma_m/2)$	$\begin{cases} p_{max} = \frac{1}{3}(\sigma_m + \sigma_a) \\ \tau_{max} = \frac{1}{2}\sigma_a \end{cases}$ $\begin{cases} p_{min} = \frac{1}{3}(\sigma_m - \sigma_a) \\ \tau_{min} = \frac{1}{2}\sigma_a \end{cases}$
Pure shear stress	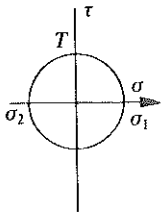	$\sigma_1 = \sigma_2$ $\sigma_3 = 0$ $T = \sigma_{1/2}$	$p(t) = 0$ $\tau(t) = \sigma_a \sin \omega t$	$\begin{cases} p_{max} = 0 \\ \tau_{max} = \sigma_a \\ p_{min} = 0 \\ \tau_{min} = -\sigma_a \end{cases}$

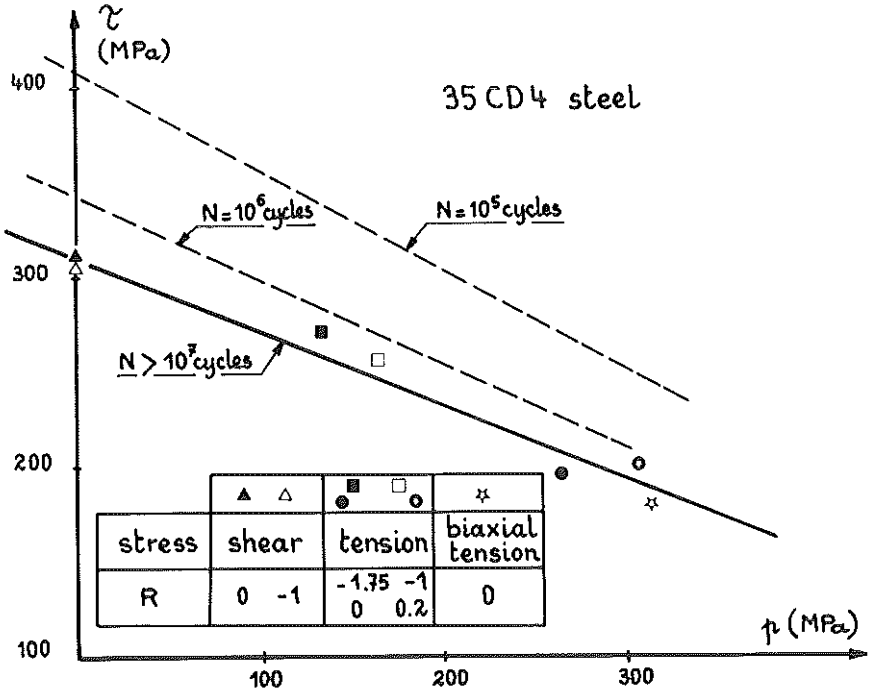

Fig 7 Dang Van diagram: damage line for a AFNOR-35 CD 4 steel

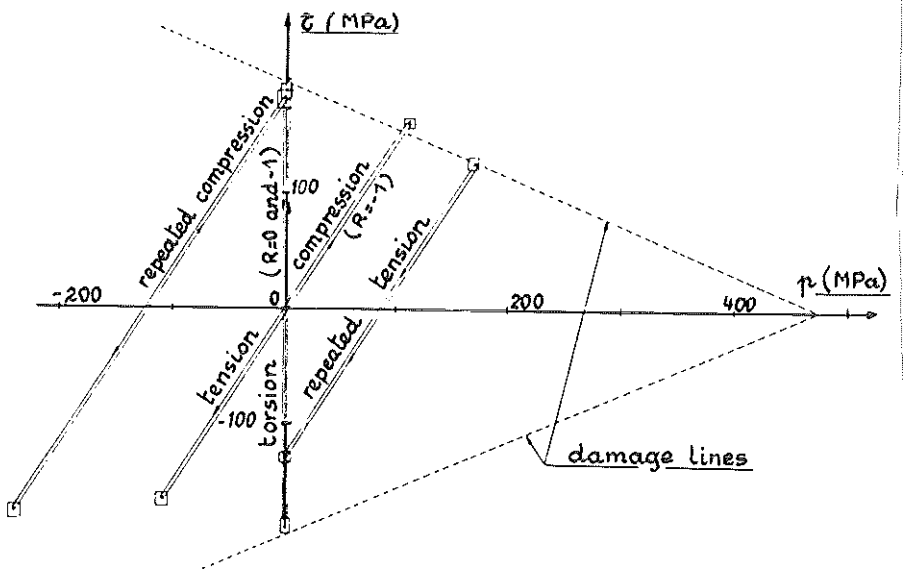

Fig 8 Dang Van diagram: damage lines for a rail steel (UTS = 850 MPa)

Fatigue tests were carried out under repeated plane bending on cylindrical bars of 36 mm diameter in steel XC42, hardened after heating by induction. To avoid the influence of the surface condition, the test pieces were machined by careful turning which led to a surface roughness before treatment of R_t = 5–7 μm.

The treatment, involving quenching after heating by induction, introduced very high residual stresses into the hardened layer, resulting in an increase in the volume of the martensitic structure in relation to the ferrite–pearlite structure of the annealed condition. In a cylindrical bar, the stress condition introduced is complex and on the surface one generally observes a tangential residual stress equal to or greater than the longitudinal residual stress (Fig. 9).

For each treatment examined, residual stress measurements were carried out on specimens subjected to $5 \cdot 10^6$ fatigue cycles under a load corresponding to the fatigue limit of each treatment. As fatigue failures are initiated on the surface of the specimens, the measurements were carried out on the surface. It is in fact the surface stress condition which determines the fatigue behaviour in this case. Measurements were carried out using X-rays. For each specimen investigated, we measured a longitudinal residual stress (σ_{Rl}) and a tangential residual stress (σ_{Rt}). Table 4 gives the different results obtained for the four treatments.

To carry out a fatigue behaviour calculation accounting for residual stresses, it is necessary first of all to know the fatigue strength of the steel making up the hardened layer in the absence of residual stresses. For this reason, fatigue tests

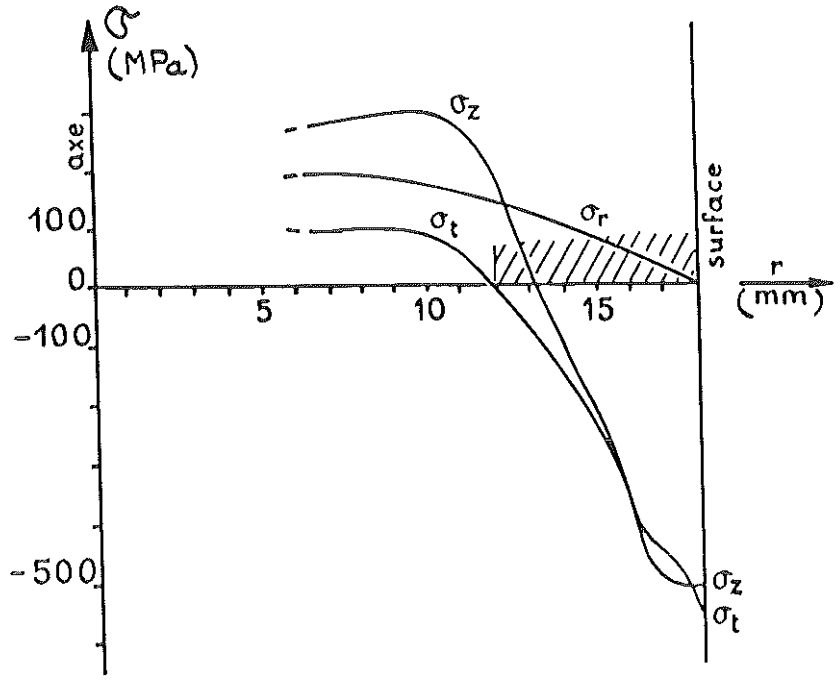

Fig 9 Residual stress gradients after a surface hardening treatment by induction (superficial hardness: HRC 54). σ_z, σ_t, and σ_r are, respectively, axial, tangential, and radial stresses

Table 4 Characteristics of various superficial hardening treatments

Ref.	*Heat treatment thickness** (*mm*)	*Surface hardness* (*Rc*)	*Endurance limit†* (*MPa*)		*Stabilized residual stress* (*MPa*)	
			σ_m	σ_a	σ_{Rl}	σ_{Rt}
A	Induction, 2.7	55–56	596	584	−128 −243	−468 −471
B	Induction, 4.2	55–56	623	610	−273 −341	−583 −676
C	Induction, 4.7	54–59	670	660	−655	−603
D	Water quenching after massive heating, 3.5	60–61	780	750	−863 −777	−1132 −1156

* Thickness for hardness higher than 45 Rc.
† $\sigma_D = \sigma_m + \sigma_a$ ($N \geqq 5 \cdot 10^6$ cycles).

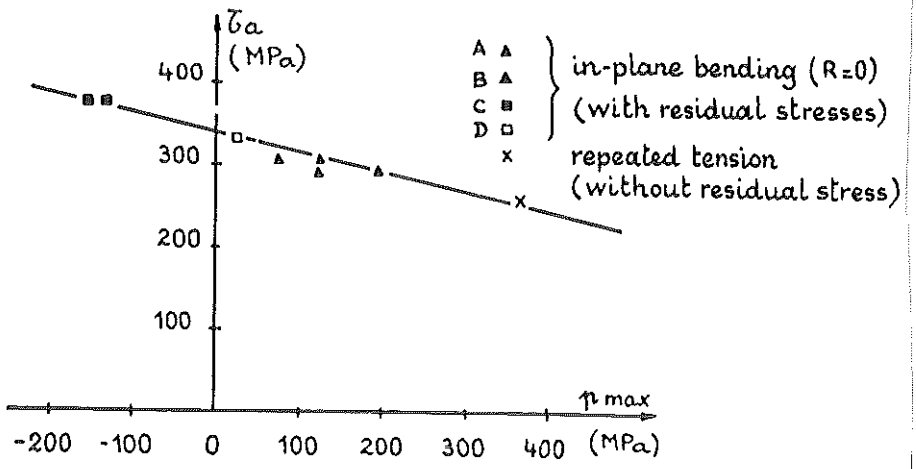

Fig 10 Analysis of the experimental results using the Dang Van criterion, in the case of residual stress gradients (surface hardening treatment)

were carried out under repeated tension on specimens of steel XC42 hardened uniformly to a hardness of 52 HRC, i.e., approaching the hardness of the treated layer, obtained by induction hardening (hardness: 54–56 R_c).

To analyse the experimental results using the Dang Van criterion, one need only introduce the following values into the diagram τ, p_{max}

$$\tau = \sigma_a/2$$
$$p_{max} = \sigma_a + (\sigma_m + \sigma_{RI} + \sigma_{Rt})/3 \tag{23}$$

One thus obtains a good distribution of the experimental points according to a linear law (Fig. 10). All the points corresponding to the induction-treated specimens and involving high residual stresses follow the same law as the point corresponding to the reference test under repeated tension on specimens without residual stresses.

The line having the equation $\tau = 342 - 0.22p_{max}$ represents the fatigue behaviour law of the steel XC42 treated to a hardness of 52–55 R_c. The different experimental points fall on this line according to the level of the residual stresses introduced by the different treatments.

Industrial applications

Fatigue behaviour of engine crankshafts

The application of the Dang Van criterion makes it possible to predict the risk of failure in automotive engine crankshafts by means of local stress measurements. Strain gauges are fixed in the transition radii of the crankpins on the flywheel side. This zone is the most highly loaded. The stress concentration

Table 5 Comparison between actual and calculated lives

Engine speed (r/min)	*Number of damaging cycles per revolution*	*Life in hours*	
		Endurance test	*Measurements and predictions*
5000	1	80	66
5200	6	10	21

factors are 2.1 under bending and 1.5 under torsion, according to Peterson (**9**). The signals obtained by these gauges make it possible to determine the local bending and torsion stresses as well as the main stresses, from which it is possible to derive the load path (τ, p), this load path being defined for four engine revolutions.

During the development of new engines, good agreement was found between predictions based on these measurements and endurance tests on the engine test bench. For example, for a diesel engine having a 2.1 litre displacement with a conventional flywheel, no failure is obtained, whereas with a heavy experimental flywheel improving the performance of the drive system, the results in Table 5 were obtained.

Figure 11 provides an example of a load path for an engine speed higher than 5000 r/min. It intersects the damaging lines determined for 10^7 cycles. In spite of the imperfection of the measurements, the approximations used with regard to the properties of the examined zone and the damage accumulation law (Miner's law), the application of the criterion allows a good evaluation of in-service performance.

Fatigue behaviour of rails

The Dang Van criterion was applied to the case of rail steels described previously. Figure 12 shows the complex cycles corresponding to the passage of a railway vehicle wheel of 1250 mm diameter (new tyre) loaded to 180 kN on a UIC 60 profile rail (mass equal to 60 kg/m) placed on a track with a modulus of $4 \cdot 10^7$ N/m^2 (**10**).

For the type of loading considered, the complex load paths undergone by the rail were plotted by means of a computer at points located at different depths in the rail head. In fact, we plotted on the ordinate the local shear stress amplitude τ_{30} calculated on planes inclined 30 degrees relative to the vertical. The study showed that what was in fact involved was the most unfavourably oriented planes, i.e., those on which the shear stress amplitude was at its maximum. This inclination is in agreement with the mean plane of fatigue crack growth ('tache ovale').

It is noted that complex cycles are located within the range of hydrostatic compression. As could be expected, the stresses are greater on the surface than

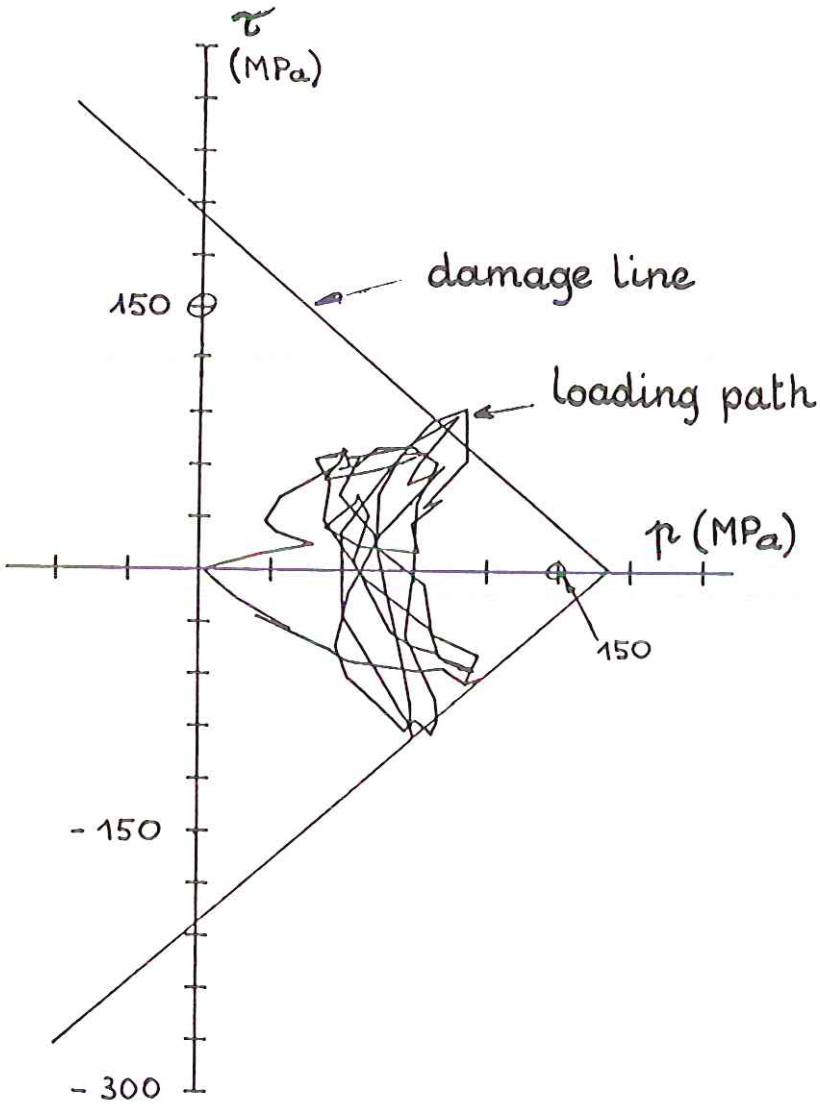

Fig 11 Loading path for a car engine crank shaft

in depth. The plotting of these cycles in the plane of the criterion, for a large number of loading cases, made it possible to arrive at the following conclusions.

(a) Increasing the wheel load has an unfavourable effect on the surface and in stress system depth.
(b) Decreasing the wheel diameter is harmful, and has a greater influence on the surface than in stresses depth.

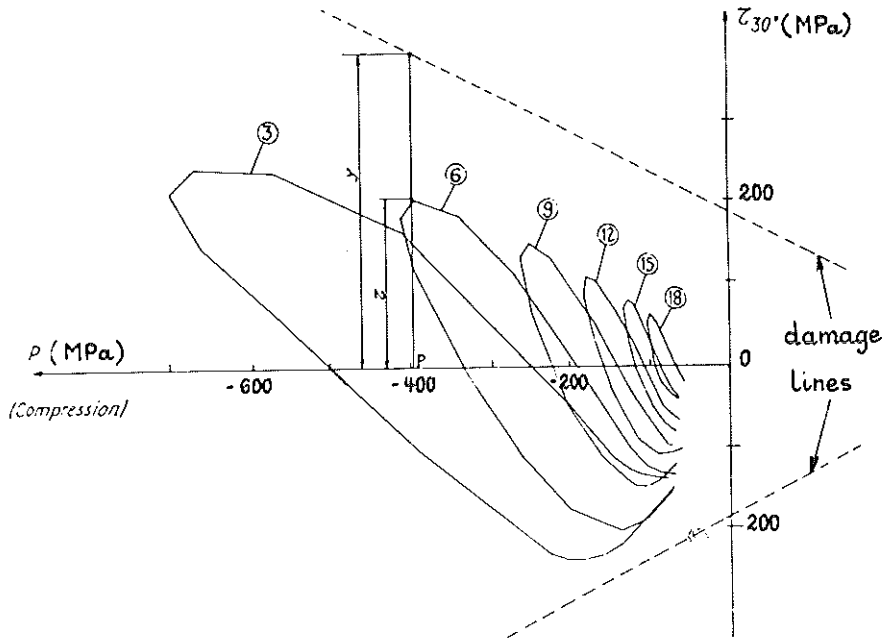

Fig 12 Complex loading paths calculated at various depths under the running rail surface and plotted on the Dang Van diagram, e.g., $\bar{3}$ means: depth equal to 3 mm

(c) A tyre having a transverse wear profile (concave) is very unfavourable, especially on the surface, and especially in the case of small wheels.

(d) Residual stresses have a favourable effect on the surface where high hydrostatic compression prevails: they shift the cycles towards the hydrostatic compressions, thus moving them away from the damaging lines. On the other hand, in depth, within a zone which corresponds substantially to that in which 'tache ovales' originate, it is the opposite which occurs since the hydrostatic pressure in the zone exhibits a tension peak.

(e) Stresses of thermal origin act as residual stresses, translating the complex cycles parallel to the axis of the ps and are thus favourable in the summer and unfavourable in the winter.

(f) A reduction in rail inertia or track rigidity has a modest but favourable influence, since it increases the flexing and hence the compression of the rail head. We have already stated that these reductions were favourable with respect to dynamic overloads. However, a rail with a high inertia spreads the bearing pressures more on the ballast and thus contributes to the maintaining of the geometrical quality of the track, also reducing dynamic overloads. Also, a heavier new rail would exhibit geometrical defects of greater wavelength. Considering the relative importance of the contradictory effects involved, it may be stated that the best solution is a heavy rail placed on a flexible support.

Conclusions

This study has made it possible to define a three-dimensional criterion concerning the fatigue limit based on the evaluation of microscopic stresses in the stabilized state. This criterion meets the requirements for obtaining realistic calculations. In particular, it has the following characteristics.

(1) It is intrinsic, i.e., it does not depend on the choice of the system coordinates.
(2) It is characteristic of the load path: the local stress $\sigma(t)$ or the strain $\varepsilon(t)$ which are the source of the damage are known by this method at each instant of the loading sequence.
(3) It can represent all the load paths which were investigated experimentally.

Such a criterion is described and corroborated by laboratory test results. Moreover, its use in the case of industrial applications corresponding to complex 3-dimensional loading shows good agreement between predictions established by means of the criterion and real in-service behaviour.

References

(1) DANG VAN, K. (1973) Sur la résistance à la fatigue des métaux, *Sciences Techniques Armement*, **47**, 3ème Fasc. Mémorial de l'Artillerie Française, Paris, Imprimerie Nationale.
(2) DANG VAN, K. (1974) Comportement à la fatigue des métaux, *Plasticité et Viscoplasticité* (Edited by RADENKOVIC, D. and SALENÇON, J.), McGraw-Hill, New York, pp. 69–72.
(3) DANG VAN, K., GRIVEAU, B., and MESSAGE, O. (1985) On a new multiaxial fatigue criterion; theory and application, *2nd Int. Conf. on Biaxial/Multiaxial Fatigue*, Sheffield, UK.
(4) GARUD, Y. S. (1981) Multiaxial fatigue: a survey of the state of the art, *J. Testing Evaluation*, **9**, 165–178.
(5) SINES, G. and OHGI, G. (1981) Fatigue criteria under combined stresses or strains, *Trans ASME*, **103**, 82–90.
(6) CROSSLAND, G. (1956) Effect of large hydrostatic pressures on the torsional fatigue strength of an alloy steel, *Proc. of the Int. Conf. of Fatigue of Metals*, I. Mech., London, pp. 138–149.
(7) FUCHS, H. O. (1979) Fatigue research with discriminating specimens, *Fatigue Engng Mater. Structures*, **2**, 207–215.
(8) LIEURADE, H. P., BASTENAIRE, F., REGNIER, L., DANG VAN, K., and LIGERON, J. C. (1982) Comportement en fatigue sous sollicitations complexes, *Mém. Sci. Rev. Mét.*, **9**, 500.
(9) PETERSON, (1974) Stress concentration factors, *Wiley Interscience*, New York, publication 98.
(10) PRASIL, P. (1976) Le comportement à la fatigue du métal du champignon des rails, *Informations Techniques SNCF*, **12**, 11–23.